The All-Seeing Eye of Resonant Auger Electron Spectroscopy: A Study on Aqueous Solution Using Tender X-Rays

Tsveta Miteva,[*,†] Nikolai V. Kryzhevoi,[‡] Nicolas Sisourat,[†] Christophe Nicolas,[¶] Wandared Pokapanich,[§] Thanit Saisopa,[‖] Prayoon Songsiriritthigul,[‖] Yuttakarn Rattanachai,[⊥] Andreas Dreuw,[#] Jan Wenzel,[#] Jérôme Palaudoux,[†] Gunnar Öhrwall,[@] Ralph Püttner,[△] Lorenz S. Cederbaum,[‡] Jean-Pascal Rueff,[†,¶] and Denis Céolin[*,¶]

†*Sorbonne Université, CNRS, Laboratoire de Chimie Physique Matière et Rayonnement, UMR 7614, F-75005 Paris, France*

‡*Theoretische Chemie, Physikalisch-Chemisches Institut, Universität Heidelberg, Im Neuenheimer Feld 229, D-69120 Heidelberg, Germany*

¶*Synchrotron SOLEIL, l'Orme des Merisiers, Saint-Aubin, F-91192 Gif-sur-Yvette Cedex, France*

§*Faculty of Science, Nakhon Phanom University, Nakhon Phanom 48000, Thailand*

‖*School of Physics, Suranaree University of Technology, Nakhon Ratchasima 30000, Thailand*

⊥*Department of Applied Physics, Faculty of Sciences and Liberal Arts, Rajamangala University of Technology Isan, Nakhon Ratchasima 30000, Thailand*

#*Interdisciplinary Center for Scientific Computing, Ruprecht-Karls University, Im Neuenheimer Feld 205A, D-69120 Heidelberg, Germany*

@*MAX IV Laboratory, Lund University, P.O. Box 118, SE-22100 Lund, Sweden*

△*Fachbereich Physik, Freie Universität Berlin, Arnimallee 14, D-14195, Berlin, Germany*

E-mail: miteva.tsveta@gmail.com; denis.ceolin@synchrotron-soleil.fr

Abstract

X-ray absorption and Auger electron spectroscopies are demonstrated to be powerful tools to unravel the electronic structure of solvated ions. In this work for the first time we use a combination of these methods in the tender x-ray regime. This allowed us to address electronic transitions from deep core levels and to probe environmental effects, specifically in the bulk of the solution since the created energetic Auger electrons possess large mean free paths. In the considered exemplary aqueous KCl solution the solvated isoelectronic K^+ and Cl^- ions exhibit notably different Auger electron spectra as a function of the photon energy. The differences appear due to dipole-forbidden transitions in aqueous K^+ whose occurrence, according to the performed *ab initio* calculations, becomes possible only in the presence of solvent water molecules.

Graphical TOC Entry

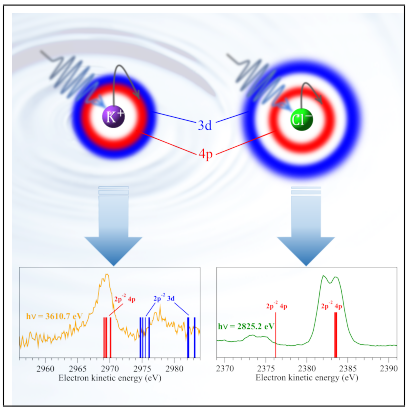

Keywords

Solvated ions, Auger electron spectroscopy, x-ray absorption spectroscopy

Understanding how atoms or molecules respond to irradiation with x-rays gives insight into the structure of solutions (Ref.[1] and references therein), and the mechanisms of radiation damage[2–4]. Depending on the photon energy, the absorption of an x-ray photon results in the population of core-excited or core-ionized states. The relaxation of these highly energetic states involves an ultrafast cascade of intraatomic processes, such as radiative and Auger decays, and it depends on the character of the initially populated states[5–12]. Furthermore, if the initially excited or ionized species is embedded in an environment, interatomic processes are possible[4,13–16].

X-ray absorption spectroscopy (XAS) in the soft x-ray regime is a powerful tool to describe core-excited states of a specific atom and thus to probe the local environment by its influence on the electronic structure. In the tender and hard x-ray regimes, these core-excited states overlap significantly due to the lifetime broadening, rendering an observation of the influence of the environment difficult. This challence can be overcome by detecting the electrons originating from the subsequent resonant Auger decay, which allows to separate the overlapping states[17,18]. With our recently commissioned microjet setup dedicated to the study of liquids by by electron spectroscopy techniques using tender x-rays[19,20], we are now able to probe much deeper core levels and corresponding fast Auger electrons. This allows us to focus our investigations on the liquid bulk by strongly reducing the specific interface contributions, and also to access ultrafast dynamical processes owing to the very short lifetimes of the corresponding core-excited states.

In this work we combine Auger electron spectroscopy (AES) together with XAS in the tender x-ray regime to study the electronic decay processes following x-ray absorption of aqueous potassium chloride at the K-edges of both K^+ and Cl^-. In particular, we demonstrate experimentally that at photon energies below the K-edges of the two ions, core-excited states are populated. These states undergo resonant Auger decay within less than 1 fs[16]. Although the K^+ and Cl^- ions are isoelectronic, they have different fingerprints in the resonant Auger spectra. We demonstrate that these differences result to a large extend from different

electronic structures of the two ions, thus confirming that the combination of XAS and AES techniques is a sensitive probe of the electronic structure of solutions.

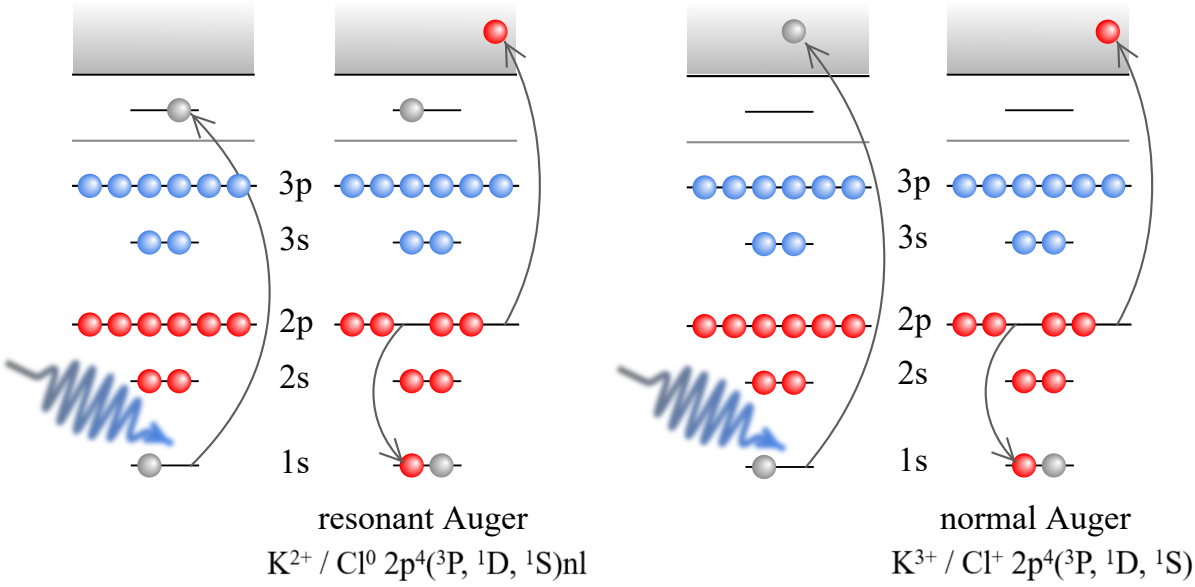

Figure 1: Schematic representation of the resonant (left) and normal (right) Auger processes of the isoelectronic K^+ and Cl^- ions.

The resonant and normal Auger spectra of K^+_{aq} and Cl^-_{aq} were measured using a newly operational microjet setup designed for the HAXPES end station of the GALAXIES beamline at the synchrotron radiation facility SOLEIL in France[19,20]; for details, see Supplementary Information (SI). Figs. 2 and 3 show these photon-energy dependent spectra as 2D maps where the abscissa reprents the Auger energy and the ordinate the photon energy; the Auger intensities are illustrated by a color code. The investigated Auger processes are schematically shown on Fig. 1. The $KL_{2,3}L_{2,3}$ normal Auger decay leads to a population of the $2p^{-2}(^3P, ^1D, ^1S)$ final states. For both, K^+ and Cl^- the observed transitions corresponding to the $2p^{-2}(^1D, ^1S)$ final states are indicated in Figs. 2(a) and 3(a). In addition, the $2p^{-2}(^1D)$ main line of K^+ exhibits a low-energy shoulder labeled A in Fig. 2(a) which will be discussed further below. Close to threshold the $KL_{2,3}L_{2,3}$ normal Auger lines are asymmetric, see Figs. 2(c) and 3(c) and also shifted to higher kinetic energies as compared to the spectra reported in[16]. This is due to post-collision interaction[21,22], which is discussed in more detail in the

SI.

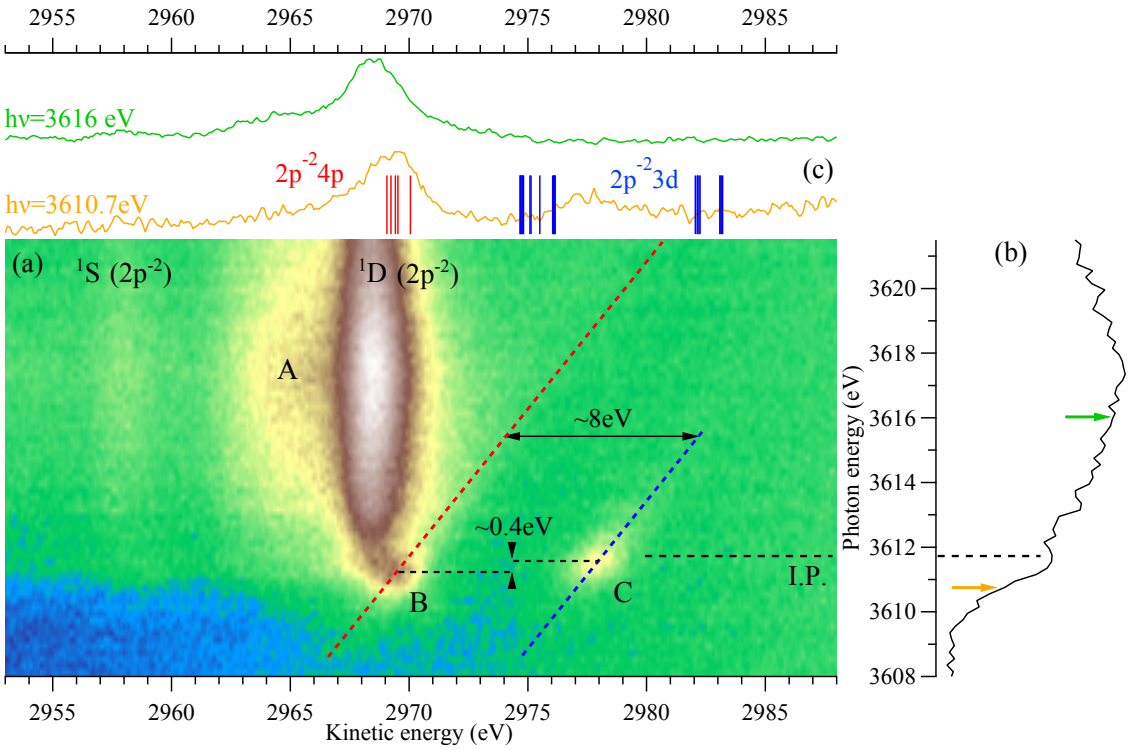

Figure 2: (a) 2D map showing the kinetic energy of the electrons emitted in $KL_{2,3}L_{2,3}$ Auger decay vs the photon energy in the vicinity of the K-edge of aqueous K^+. The features A, B and C are discussed in the text. (b) Experimental partial electron yield spectrum of K^+ obtained after integrating over the kinetic energies of the Auger electrons. (c) Auger spectra at photon energies 3610.7 eV and 3616 eV. The vertical bars in the resonant Auger spectrum measured at 3610.7 eV indicate the spectator Auger energies of the calculated doublet $2p^{-2}$ 3d (blue) and $2p^{-2}4p$ (red) states of $K^+(H_2O)_6$.

In the pre-edge regions of the XA spectra **I use XA spectra instead of XAS (x-ray absorption spectroscopy) spectra since for me spectroscopy spectra sounds really weird. But you can go back to XAS if you really want.** of K^+ and Cl^- shown, see Figs. 2(b) and 3(b), no core-excited states are visible due to their lifetime broadening and energetic proximity to the ionization threshold. They can, however, be observed by their resonant Auger features, which disperse with photon energy and are indicated by dashed diagonal lines in Figs. 2(a) and 3(a). To assign these features, calculations of the XA spectra and the Auger final states were performed.

The XA spectra in the region of the lowest core-excited states of the isolated K^+ and

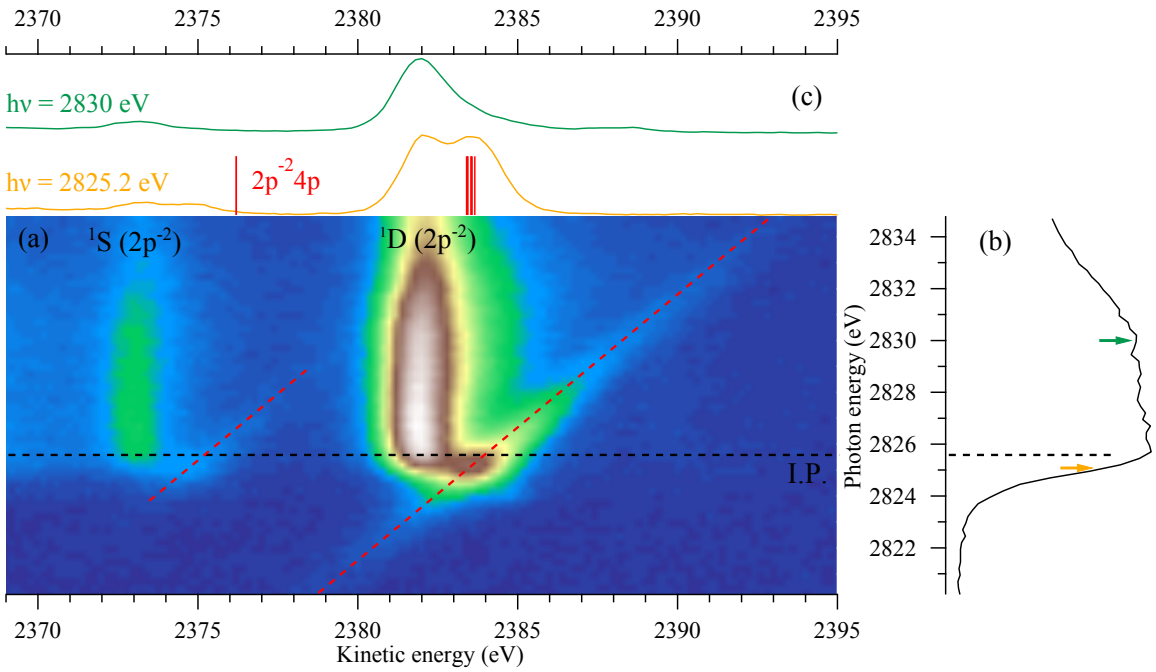

Figure 3: (a) 2D map showing the kinetic energy of the electrons emitted in $KL_{2,3}L_{2,3}$ Auger decay vs the photon energy in the vicinity of the K-edge of aqueous Cl^-. (b) Experimental partial electron yield spectrum of Cl^- obtained after integrating over the kinetic energies of the Auger electrons. (c) Auger spectra at photon energies 2825.2 eV and 2830.0 eV. The vertical bars in the resonant Auger spectrum at 2825.2 eV indicate the the spectator Auger energies of the calculated doublet $2p^{-2}4p$ states of $Cl^-(H_2O)_6$.

Cl^- ions and their hexa-coordinated clusters representing K^+_{aq} and Cl^-_{aq} where calculated. For this we used the algebraic diagrammatic construction method for the polarization propagator[23] within the core-valence separation approximation[24–26] (CVS-ADC(2)x) as implemented in the Q-Chem package[27–30] (see SI for details). The theoretical XAS spectra of the isolated ions (Fig. 4(a),(b)) show the two dipole-allowed states, $1s^{-1}4p$ and $1s^{-1}5p$, which are split by 4.3 eV and 10.8 eV in K^+ and Cl^-, respectively. For both ions, the energy positions of the dipole-forbidden $1s^{-1}3d$ state is marked with blue crosses. Its different relative position in K^+ and $Cl^-$is for understanding the Auger spectra of the two ions as discussed below. Upon addition of water molecules, the degeneracy of the states is lifted and they interact with other states of the ion or the neighboring water molecules (Fig. 4(c),(d)). Thus, dipole-forbidden states acquire intensity in the cluster. A similar effect was observed in the XAS spectra of microsolvated clusters of Na^+ and Mg^{2+}[31].

In detail, in the XA spectrum of the 6-coordinated K^+ cluster the lowest peak in the spectrum contains three states (Fig. 4(c)). The lowest- and highest-lying states are split by approximately 0.5 eV and they have mixed 4p and 5p character while the low-intensity state in between has a predominantly $1s^{-1}3d$ character. In the hexa-coordinated cluster of Cl^-, the solvent molecules have little influence on the position and character of the first state – it has mainly Cl^- $1s^{-1}4p$ character with some admixture of states of the nearest water molecules (Fig. 4(d)).

We also computed the lowest doublet states of the type $K^{2+}[2p^{-2}nl](H_2O)_6$ and $Cl^0[2p^{-2}nl](H_2O)_6$ representing the final states of the spectator Auger decay , which is the predominant decay process for the low-lying core-excited states in isoelectronic argon[32]. The calculations were performed at the Configuration Interaction Singles (CIS) level using the GAMESS-US package[33–35] (see SI for details). The energy positions of the states (see bars on Figs. 2(c) and 3(c)) are adjusted to the kinetic-energy scale of the Auger spectra of both ions such that the lowest $2p^{-2}(^1D)4p$ states coincide with the maxima of the dipsersive features related to the ^1D main line.

In the following we shall assign the spectral features visible in the 2D maps. In the 2D map of Cl^- (Fig. 3(a)) two dispersive resonant Auger features are visible and indicated with diagonal dashed lines. Both of them exhibit a maximum at $h\nu = 2825.2$ eV, i.e. $\cong$ 400 meV (number has to be checked) below the ionization threshold. This value agrees well with the calculated position of the $1s^{-1} \rightarrow 4p$ excitation in 6-koordinated Cl^-, see Fig. 4(d), which has some admixtures of the states of the nearest water molecules. Moreover, the maxima in the kinetic energies of these dispersive features are split by $\cong$ 8.5 eV, which is in line with the calculated values for the $2p^{-2}(^1S)4p$ and $2p^{-2}(^1D)4p$ final states of $\cong$ 7 eV. Consequently, we assign these features as caused by $1s^{-1}4p$ excitations which subsequently decay by resonant Auger to the $2p^{-2}(^1S, ^1D)4p$ final states.

The 2d-map of K^+shown in Fig. 2(a) also displays 2 dispersive features, which are indicated with dashed lines. The line denoted as B exhibit its maxima at hν = 3611.2 eV

and $E_{\mathrm{kin}} = 2969.2\,\mathrm{eV}$ while the line labeled C exhibit the maximum at $h\nu = 3611.6\,\mathrm{eV}$ and $E_{\mathrm{kin}} = 2978.1\,\mathrm{eV}$. The observed and calculated energy positions relative to the K^+1s^{-1} threshold in combination with the relative energy position of the $2p^{-2}nl$ states suggest that feature B is caused by a $1s \rightarrow 4p$ exciation with a subsequent resonant Auger decay to a $2p^{-2}(^1D)4p$ final state and feature C is by a $1s \rightarrow 3d$ exciation with a subsequent resonant Auger decay to a $2p^{-2}(^1D)3d$ final state. This assignment is supported by the low intensity of the latter feature, which is dipole-forbidden in the isolated ion.

It is also supported by the energy difference between the spectral features A and C, which matches well the lowest ionization potential of liquid water of $I_{aq} \cong 11.16$ eV.[36] Feature A is assigned to a charge transfer from a water molecule W to the 3d orbital of the K-ion during the Auger decay, i.e. $K^{2+}(1s^{-1} \rightarrow K^{2+}(2p^{-2}3d)W^{+}$[16], so that its energy position should be lower by I_{aq} if the very small energy distance of the $1s \rightarrow 3d$ exciation from threshold is considered. Due to the high intensity of shoulder A no dispersive features related to the $2p^{-2}(^1S)$ parent state are observed in the 2d-map of K^+.

Finally we want to point out that the resonances of K^+_{aq} and Cl^-_{aq} calculated to be above the correspoinding ionization threshold, see Fig. 4(c,d), are not observed. This might be due to the fact that the corresponding resonant Auger spectra are energetically too close to the more intense normal Auger main lines.

The delocalization of core-excited electrons in aqueous solutions is ultrafast and as such it competes with the resonant Auger decay[38,39]. To estimate the delocalization time of the core-excited electron, τ_{CT}, at the pre-edges of K^+ and Cl^-, we used the core-hole clock method.[17,40–43] Our analysis, presented in detail in SI, shows that in the case of Cl^-, τ_{CT} is of the same order as the Auger lifetime, i.e. $\sim$1 fs. The treatment is more complex in the K^+ case due to the presence of multiple competing processes. However, one can expect much less efficient delocalization in K^+ because the core-excited states appear 1.2 eV below the ionization threshold compared to 0.2 eV for chloride and, moreover, the lifetime of the K1s core hole is shorter than for chloride (0.9 vs. 1 fs).

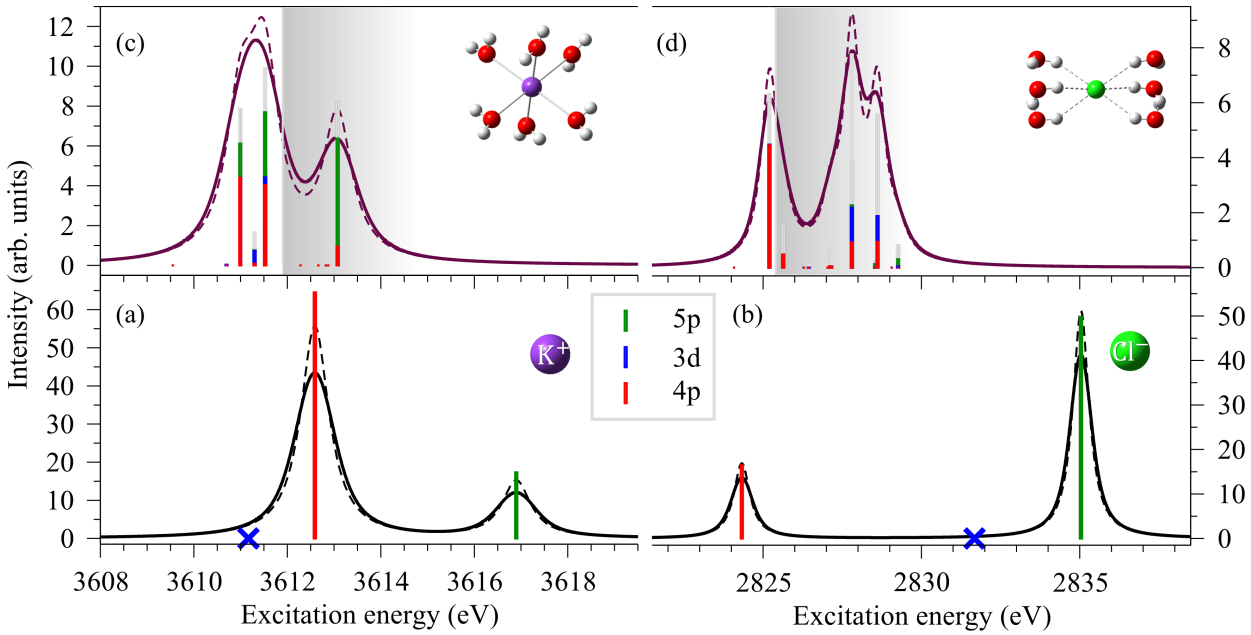

Figure 4: XAS spectra of the lowest K-shell resonant transitions in the isolated K^+ (a) and Cl^- (b) ions and their 6-coordinated clusters, (c) and (d). For comparison with the experiment, the theoretical stick spectra are convolved with a Lorentzian of FWHM 0.74 eV and 0.62 eV representing the lifetime broadening of K^+ and Cl^- [37] (dashed lines) and a Voigt profile (solid line) to account for both the lifetime and the experimental broadening (see text). The colors in the stick spectrum represent the projections of the singly-occupied natural orbitals (SONOs) of the core-excited 6-coordinated clusters on the basis of SONOs belonging to the $1s^{-1}3d$, $1s^{-1}4p$, and $1s^{-1}5p$ states of the isolated ions. The remaining contributions from higher-lying atomic core excitations or from excitations to the solvent molecules are depicted as grey sticks. The theoretical XAS spectra of both K^+ and Cl^- were shifted to higher photon energies such that the energies of the lowest core-excited states correspond to the experimentally determined ones. The experimental ionization thresholds are depicted as grey boxes.

In summary, we studied the electronic structure of aqueous solution of KCl at the K-edges of both K^+_{aq} and Cl^-_{aq} by combining XAS and AES in the tender x-ray regime, and *ab initio* calculations. The Auger electron spectra of both ions exhibit features of normal and resonant Auger processes. The spectator resonant Auger decay following the $1s^{-1}4p$ excitation proceeds similarly for both aqueous K^+ and Cl^- resulting in dispersive lines with maxima close to the normal Auger features. However, there is a clear difference between the two ions due to the non-negligible excitation of the dipole-forbidden $1s^{-1}3d$ state of K^+ in solution. The spectator Auger decay of this state produces an additional feature which is

well separated from the remaining Auger features. These results are an important first step in the study of relaxation cascades triggered by x-ray photoabsorption in liquids. The Auger processes considered here are inevitably followed by multiple intra- and interatomic electronic decays, such as interatomic Coulombic decay (ICD) and electron-transfer mediated decay (ETMD)[4,15]. As a result of the latter processes, genotoxic free radicals and slow electrons are formed in the vicinity of the metal center. The magnitude of the damage inflicted upon the environment and the energies of the emitted electrons depend on the initial Auger step, and can therefore be controlled by tuning the energy of the radiation. Consequently, the results of this work can have implications in understanding radiation chemistry and radiation damage in biologically relevant systems in which metallic centers are ubiquitous.

Acknowledgement

We thank Prof. Nobuhiro Kosugi and Dr. Matjaž Žitnik for the fruitful discussions. Experiments were performed at the GALAXIES beamline, SOLEIL Synchrotron, France (Proposal No. 20140160). The authors are grateful to the SOLEIL staff for assistance during the beamtime. This project has received funding from the Research Executive Agency (REA) under the European Union's Horizon 2020 research and innovation programme Grant agreement No. 705515. Campus France and the PHC SIAM exchange program are acknowledged for financial support (project No. 38282QB). L. S. Cederbaum and N. V. Kryzhevoi acknowledge the financial support of the European Research Council (ERC) (Advanced Investigator Grant No. 692657) and the Deutsche Forschungsgemeinschaft (DFG research unit 1789).

Supporting Information Available

- suppinfo.pdf: contains 1) a detailed description of the experiment, as well as the *ab initio* calculations; 2) an explanation of the post-collision interaction shift observed in the experimental Auger spectra; 3) the radial density distributions of the core excited

states of the bare ions; 4) the partial cross sections and charge transfer time extracted from the experimental 2D map near the Cl1s edge.

References

(1) Smith, J. W.; Saykally, R. J. Soft X-ray Absorption Spectroscopy of Liquids and Solutions. *Chem. Rev.* **2017**, *117*, 13909–13934.

(2) O'Neill, P.; Stevens, D. L.; Garman, E. F. Physical and chemical considerations of damage induced in protein crystals by synchrotron radiation: a radiation chemical perspective. *J. Synchrotron Radiat.* **2002**, *9*, 329–332.

(3) Carugo, O.; Carugo, K. D. When X-rays modify the protein structure: radiation damage at work. *Trends Biochem. Sci.* **2005**, *30*, 213–219.

(4) Stumpf, V.; Gokhberg, K.; Cederbaum, L. S. The role of metal ions in X-ray-induced photochemistry. *Nat. Chem.* **2016**, *8*, 237–241.

(5) Stoychev, S. D.; Kuleff, A. I.; Tarantelli, F.; Cederbaum, L. S. On the interatomic electronic processes following Auger decay in neon dimer. *J. Chem. Phys.* **2008**, *129*, 074307.

(6) Demekhin, P. V.; Scheit, S.; Stoychev, S. D.; Cederbaum, L. S. Dynamics of interatomic Coulombic decay in a Ne dimer following the $K{-}L_1L_{2,3}(^1P)$ Auger transition in the Ne atom. *Phys. Rev. A* **2008**, *78*, 043421.

(7) Demekhin, P. V.; Chiang, Y.-C.; Stoychev, S. D.; Kolorenč, P.; Scheit, S.; Kuleff, A. I.; Tarantelli, F.; Cederbaum, L. S. Interatomic Coulombic decay and its dynamics in NeAr following K-LL Auger transition in the Ne atom. *J. Chem. Phys.* **2009**, *131*, 104303.

(8) Ouchi, T.; Sakai, K.; Fukuzawa, H.; Higuchi, I.; Demekhin, P. V.; Chiang, Y.-C.;

Stoychev, S. D.; Kuleff, A. I.; Mazza, T.; Schöffler, M. et al. Interatomic Coulombic decay following Ne 1s Auger decay in NeAr. *Phys. Rev. A* **2011**, *83*, 053415.

(9) Miteva, T.; Chiang, Y.-C.; Kolorenč, P.; Kuleff, A. I.; Cederbaum, L. S.; Gokhberg, K. The effect of the partner atom on the spectra of interatomic Coulombic decay triggered by resonant Auger processes. *J. Chem. Phys.* **2014**, *141*, 164303.

(10) Travnikova, O.; Marchenko, T.; Goldsztejn, G.; Jänkälä, K.; Sisourat, N.; Carniato, S.; Guillemin, R.; Journel, L.; Céolin, D.; Püttner, R. et al. Hard-X-Ray-Induced Multistep Ultrafast Dissociation. *Phys. Rev. Lett.* **2016**, *116*, 213001.

(11) Gokhberg, K.; Kolorenč, P.; Kuleff, A. I.; Cederbaum, L. S. Site- and energy-selective slow-electron production through intermolecular Coulombic decay. *Nature* **2014**, *505*, 661–663.

(12) Trinter, F.; Schöffler, M. S.; Kim, H.-K.; Sturm, F. P.; Cole, K.; Neumann, N.; Vredenborg, A.; Williams, J.; Bocharova, I.; Guillemin, R. et al. Resonant Auger decay driving intermolecular Coulombic decay in molecular dimers. *Nature* **2014**, *505*, 664–666.

(13) Pokapanich, W.; Bergersen, H.; Bradeanu, I. L.; Marinho, R. R. T.; Lindblad, A.; Legendre, S.; Rosso, A.; Svensson, S.; Björneholm, O.; Tchaplyguine, M. et al. Auger Electron Spectroscopy as a Probe of the Solution of Aqueous Ions. *J. Am. Chem. Soc.* **2009**, *131*, 7264–7271.

(14) Pokapanich, W.; Kryzhevoi, N. V.; Ottosson, N.; Svensson, S.; Cederbaum, L. S.; Öhrwall, G.; Björneholm, O. Ionic-charge dependence of the intermolecular Coulombic decay time-scale for aqueous ions probed by the core-hole clock. *J. Am. Chem. Soc.* **2011**, *133*, 13430.

(15) Unger, I.; Seidel, R.; Thürmer, S.; Pohl, M. N.; Aziz, E. F.; Cederbaum, L. S.; Muchová, E.; Slavíček, P.; Winter, B.; Kryzhevoi, N. V. Observation of electron-transfer-mediated decay in aqueous solution. *Nat. Chem.* **2017**, *9*, 708.

(16) Céolin, D.; Kryzhevoi, N. V.; Nicolas, C.; Pokapanich, W.; Choksakulporn, S.; Songsiriritthigul, P.; Saisopa, T.; Rattanachai, Y.; Utsumi, Y.; Palaudoux, J. et al. Ultrafast Charge Transfer Processes Accompanying KLL Auger Decay in Aqueous KCl Solution. *Phys. Rev. Lett.* **2017**, *119*, 263003.

(17) Föhlisch, A.; Feulner, P.; Hennies, F.; Fink, A.; Menzel, D.; Sanchez-Portal, D.; Echenique, P. M.; Wurth, W. Direct observation of electron dynamics in the attosecond domain. *Nature* **2005**, *436*, 373.

(18) Goldsztejn, G.; Marchenko, T.; Ceolin, D.; Journel, L.; Guillemin, R.; Rueff, J.-P.; Kushawaha, R. K.; Puttner, R.; Piancastelli, M. N.; Simon, M. Electronic state-lifetime interference in resonant Auger spectra: a tool to disentangle overlapping core-excited states. *Phys. Chem. Chem. Phys.* **2016**, *18*, 15133–15142.

(19) Céolin, D.; Ablett, J.; Prieur, D.; Moreno, T.; Rueff, J.-P.; Marchenko, T.; Journel, L.; Guillemin, R.; Pilette, B.; Marin, T. et al. Hard X-Ray Photoelectron Spectroscopy on the GALAXIES Beamline at the SOLEIL Synchrotron. *J. Electron Spectrosc. Relat. Phenom.* **2013**, *190, Part B*, 188 – 192.

(20) Rueff, J.-P.; Ablett, J. M.; Céolin, D.; Prieur, D.; Moreno, T.; Balédent, V.; Lassalle-Kaiser, B.; Rault, J. E.; Simon, M.; Shukla, A. The GALAXIES Beamline at the SOLEIL Synchrotron: Inelastic X-Ray Scattering and Photoelectron Spectroscopy in the Hard X-Ray Range. *J. Synchrotron Rad.* **2015**, *22*, 175–179.

(21) Russek, A.; Mehlhorn, W. Post-collision interaction and the Auger lineshape. *J. Phys. B At. Mol. Opt. Phys.* **1986**, *19*, 911.

(22) Guillemin, R.; Sheinerman, S.; Püttner, R.; Marchenko, T.; Goldsztejn, G.; Journel, L.; Kushawaha, R. K.; Céolin, D.; Piancastelli, M. N.; Simon, M. Postcollision interaction effects in KLL Auger spectra following argon $1s$ photoionization. *Phys. Rev. A* **2015**, *92*, 012503.

(23) Schirmer, J. Beyond the random-phase approximation: A new approximation scheme for the polarization propagator. *Phys. Rev. A* **1982**, *26*, 2395–2416.

(24) Barth, A.; Schirmer, J. Theoretical core-level excitation spectra of N_2 and CO by a new polarisation propagator method. *J. Phys. B At. Mol. Opt. Phys.* **1985**, *18*, 867.

(25) Cederbaum, L. S.; Domcke, W.; Schirmer, J. Many-body theory of core holes. *Phys. Rev. A* **1980**, *22*, 206–222.

(26) Barth, A.; Cederbaum, L. S. Many-body theory of core-valence excitations. *Phys. Rev. A* **1981**, *23*, 1038–1061.

(27) Wenzel, J.; Wormit, M.; Dreuw, A. Calculating core-level excitations and x-ray absorption spectra of medium-sized closed-shell molecules with the algebraic-diagrammatic construction scheme for the polarization propagator. *J. Comp. Chem.* **2014**, *35*, 1900–1915.

(28) Wenzel, J.; Wormit, M.; Dreuw, A. Calculating X-ray Absorption Spectra of Open-Shell Molecules with the Unrestricted Algebraic-Diagrammatic Construction Scheme for the Polarization Propagator. *J. Chem. Theory Comput.* **2014**, *10*, 4583–4598.

(29) Wormit, M.; Rehn, D. R.; Harbach, P. H.; Wenzel, J.; Krauter, C. M.; Epifanovsky, E.; Dreuw, A. Investigating excited electronic states using the algebraic diagrammatic construction (ADC) approach of the polarisation propagator. *Mol. Phys.* **2014**, *112*, 774–784.

(30) Shao, Y.; Gan, Z.; Epifanovsky, E.; Gilbert, A. T.; Wormit, M.; Kussmann, J.; Lange, A. W.; Behn, A.; Deng, J.; Feng, X. et al. Advances in molecular quantum chemistry contained in the Q-Chem 4 program package. *Mol. Phys.* **2015**, *113*, 184–215.

(31) Miteva, T.; Wenzel, J.; Klaiman, S.; Dreuw, A.; Gokhberg, K. X-Ray absorption spectra of microsolvated metal cations. *Phys. Chem. Chem. Phys.* **2016**, *18*, 16671–16681.

(32) Céolin, D.; Marchenko, T.; Guillemin, R.; Journel, L.; Kushawaha, R. K.; Carniato, S.; Huttula, S.-M.; Rueff, J. P.; Armen, G. B.; Piancastelli, M. N. et al. Auger resonant-Raman study at the Ar K edge as probe of electronic-state-lifetime interferences. *Phys. Rev. A* **2015**, *91*, 022502.

(33) Brooks, B. R.; Laidig, W. D.; Saxe, P.; Handy, N. C.; Schaefer III, H. F. The Loop-Driven Graphical Unitary Group Approach: A Powerful Method for the Variational Description of Electron Correlation. *Phys. Scr.* **1980**, *21*, 312.

(34) Brooks, B. R.; Schaefer, H. F. The graphical unitary group approach to the electron correlation problem. Methods and preliminary applications. *J. Chem. Phys.* **1979**, *70*, 5092–5106.

(35) Schmidt, M. W.; Baldridge, K. K.; Boatz, J. A.; Elbert, S. T.; Gordon, M. S.; Jensen, J. H.; Koseki, S.; Matsunaga, N.; Nguyen, K. A.; Su, S. et al. General atomic and molecular electronic structure system. *J. Comp. Chem.* **1993**, *14*, 1347–1363.

(36) Winter, B.; Weber, R.; Widdra, W.; Dittmar, M.; Faubel, M.; Hertel, I. V. Full Valence Band Photoemission from Liquid Water Using EUV Synchrotron Radiation. *J. Phys. Chem. A* **2004**, *108*, 2625–2632.

(37) Krause, M. O.; Oliver, J. H. Natural widths of atomic K and L levels, Kα X-ray lines and several KLL Auger lines. *J. Phys. Chem. Ref. Data* **1979**, *8*, 329–338.

(38) Nordlund, D.; Ogasawara, H.; Bluhm, H.; Takahashi, O.; Odelius, M.; Nagasono, M.; Pettersson, L. G. M.; Nilsson, A. Probing the Electron Delocalization in Liquid Water and Ice at Attosecond Time Scales. *Phys. Rev. Lett.* **2007**, *99*, 217406.

(39) Ottosson, N.; Öhrwall, G.; Björneholm, O. Ultrafast charge delocalization dynamics in aqueous electrolytes: New insights from Auger electron spectroscopy. *Chem. Phys. Lett.* **2012**, *543*, 1 – 11.

(40) Björneholm, O.; Nilsson, A.; Sandell, A.; Hernnäs, B.; Mrtensson, N. Determination of time scales for charge-transfer screening in physisorbed molecules. *Phys. Rev. Lett.* **1992**, *68*, 1892–1895.

(41) Karis, O.; Nilsson, A.; Weinelt, M.; Wiell, T.; Puglia, C.; Wassdahl, N.; Mårtensson, N.; Samant, M.; Stöhr, J. One-Step and Two-Step Description of Deexcitation Processes in Weakly Interacting Systems. *Phys. Rev. Lett.* **1996**, *76*, 1380–1383.

(42) Wurth, W.; Menzel, D. Ultrafast electron dynamics at surfaces probed by resonant Auger spectroscopy. *Chem. Phys.* **2000**, *251*, 141 – 149.

(43) Brühwiler, P. A.; Karis, O.; Mårtensson, N. Charge-transfer dynamics studied using resonant core spectroscopies. *Rev. Mod. Phys.* **2002**, *74*, 703–740.